Experimental Validation of an 8 Element EMAT Phased Array Probe for Longitudinal Wave Generation

Florian Le Bourdais[1, a)] and Benoit Marchand[1]

[1] *CEA LIST, Centre de Saclay F-91191 Gif-sur-Yvette, France*

[a)]Corresponding author: florian.lebourdais@cea.fr

Abstract. Sodium cooled Fast Reactors (SFR) use liquid sodium as a coolant. Liquid sodium being opaque, optical techniques cannot be applied to reactor vessel inspection. This makes it necessary to develop alternative ways of assessing the state of the structures immersed in the medium. Ultrasonic pressure waves are well suited for inspection tasks in this environment, especially using pulsed electromagnetic acoustic transducers (EMAT) that generate the ultrasound directly in the liquid sodium. The work carried out at CEA LIST is aimed at developing phased array EMAT probes conditioned for reactor use. The present work focuses on the experimental validation of a newly manufactured 8 element probe which was designed for beam forming imaging in a liquid sodium environment. A parametric study is carried out to determine the optimal setup of the magnetic assembly used in this probe. First laboratory tests on an aluminium block show that the probe has the required beam steering capabilities.

CONTEXT: INSPECTION NEEDS WITHIN THE ASTRID PROJECT

Together with its partners the French Atomic Energy Commission (CEA) has been developing a prototype Sodium cooled Fast Reactor (SFR) named ASTRID (Advanced Sodium Technical Reactor for Industrial Demonstration) since 2007. The SFR technology was chosen among the promising Generation IV systems with the objective to assess industrial capabilities of heavy waste element transmutation. This choice is motivated by the historical position of SFRs within the French nuclear program and the operational knowledge gained during the 1980s with the Rhapsodie, Phenix and Superphenix reactors. One of the goals of the ASTRID reactor concept is to attain higher safety levels than any past SFR design and at least equal to current third generation systems such as the EPR or APWR reactors (see [1]). Contrary to previous French SFRs, In-Service Inspection and Repair (ISI&R) is taken into account since the early reactor design stage as a transverse issue linking together safety analysis, economic reliability and investment protection. This includes providing enhanced inspection and maintenance systems during reactor operating life.

The liquid sodium environment is one of the most challenging aspects when designing inspection methods for SFRs, especially when compared to water cooled reactor ISI&R. Due to the opaqueness of sodium, optic inspection means cannot be used, a fact that has led to the development of numerous ultrasonic inspection methods. Sodium being also a chemically reactive substance, immersion inspection probes have to be designed with great care to avoid chemical attack. Finally, due to the thermodynamic properties of liquid sodium, the minimal temperature allowed during cold shutdown is 200°C, which is higher than usual non-destructive testing temperature conditions.

Following research efforts during the 80s and 90s, ultrasonic probes for use in liquid sodium have been developed by CEA (see [2], [3]). These probes consist of piezoelectric crystals encased in stainless steel for use in liquid sodium and modified for robust operation under temperatures as high as 500°C. However, these probes also suffer from the well-known front face wetting problem (see [4]) that restricts their usability under certain conditions. Therefore, alternative means of generating ultrasonic waves in liquid sodium have been explored at CEA in the form of electromagnetic acoustic transducer (EMAT, see [5]) based longitudinal wave probes. The main advantage for pursuing the development of these probes is the absence of wetting problems, due to the generation of pressure waves through currents induced in the sodium itself.

41st Annual Review of Progress in Quantitative Nondestructive Evaluation
AIP Conf. Proc. 1650, 1496-1505 (2015); doi: 10.1063/1.4914767

The principle of EMAT force generation applied to liquid sodium is shown in Fig. 1. A static magnetic field is induced in the liquid sodium by permanent magnets suitably oriented. The transducer coils are excited by a transient pulse and induce a time-dependent eddy current distribution in the propagation medium. The volumic Lorentz force results from the dot product between the eddy current distribution and the static magnetic field: $F_{Lorentz} = J \times B$. Due to the pulsed eddy current oscillating in time, an ultrasonic wave is emitted with frequency characteristics close to the original pulse. In liquid sodium, the ultrasonic pressure wave can then be used for inspection purposes. Potential applications include object detection, distance measurements, surface metrology, imaging for exploratory purposes and non-destructing testing of components.

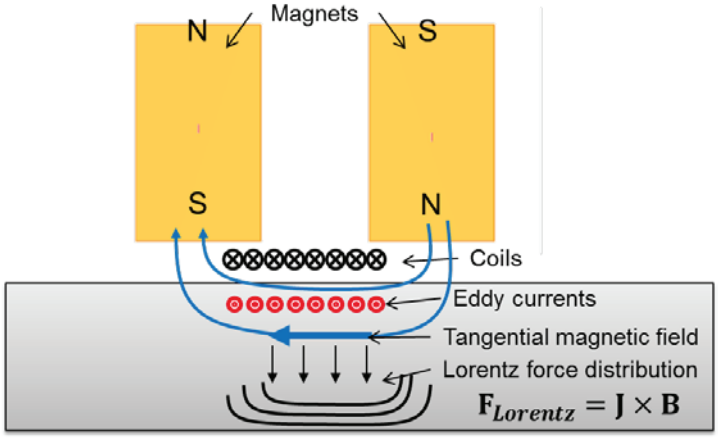

FIGURE 1. Principle of EMAT force generation applied to liquid sodium. Coils induce eddy currents in the sodium that interacts with the tangential magnetic field component created by the magnets positioned above the coils to generate a volumic Lorentz force distribution in the liquid sodium. The force gives rise to propagating pressure waves that can be used for inspection purposes.

Since 2009, several EMAT probes have been developed at CEA LIST (see [6]), with single element and more recently phased array probes up to 8 elements among them. Sodium tests have shown these probes to be compatible with shutdown reactor requirements: liquid sodium at 200°C, slow sodium flow, 30 days under sodium immersion. Moreover, one of the single element EMAT probes has been shown to be fully operational under irradiation conditions close to those encountered in the reactor vessel. It was irradiated in a linear accelerator facility at an energy of 7920 Gy/hour until reaching an integrated dose of 216 kGy. Continuous monitoring of the probe signal has shown only a slight increase in electrical noise at the end of the process and thus has proven current CEA EMAT designs to be robust to irradiated environments. To improve upon previous probes, the current objective at CEA is to develop an 8 element phased array EMAT that can electronically deflect the ultrasonic beam in a region within 100 mm of a target object. This would allow producing B-scan images for imaging tasks such as identification of components or object detection. In 2013, a first version of this probe was developed, followed by a second iteration for which coils etched on a 6 layer Kapton were ordered in 2014. To complete the design of the probe, the positioning of the two permanent magnets had to be determined. The next section explains how the position of the magnetic assembly (i.e. the two magnets shown in Fig. 1) was chosen using an optimization process.

PARAMETRIC STUDY ON OPTIMAL MAGNET POSITION USING SIMULATION TOOLS

In this section, we will explain how we chose the geometry of the magnetic part of the probe in the final probe design. The two parts of the probe, the magnetic assembly (which includes a Ferrite element to guide magnetic field lines in the space above the permanent magnet) and the coils etched on Kapton material, are shown in Fig. 2.

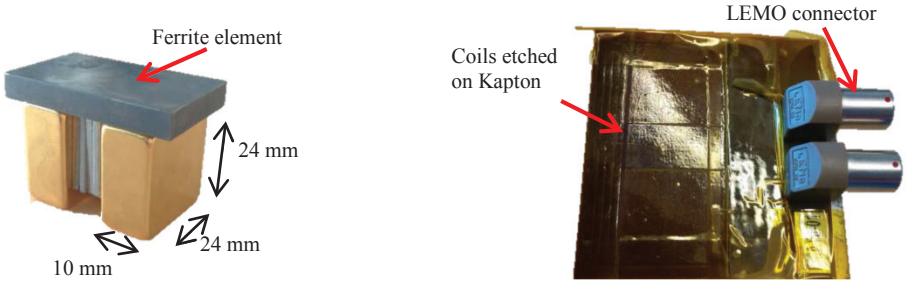

(a) (b)

FIGURE 2. Depiction of the two EMAT probe parts: magnetic assembly consisting of two permanent magnets as well as a ferrite element (a) and coils etched on Kapton with LEMO connectors (b).

The specific point that we are trying to investigate here is how the magnetic assembly can be placed most efficiently on top of the coil element of the probe for the generation of longitudinal waves. In principle, the two magnets can be positioned relatively to the coils in an infinite number of ways. However, due to the symmetry of the coil design, it seems reasonable to choose a way of positioning them that follows the same symmetry. This introduces a first parameter to our study: the magnet separation distance (which is chosen to be symmetric with respect to the center of our coil design). We also select a second parameter to describe the position of the magnetic part of the probe: the lift-off of the magnetic assembly relatively to the coils that we will simply call lift-off. These two parameters are illustrated in the figure below:

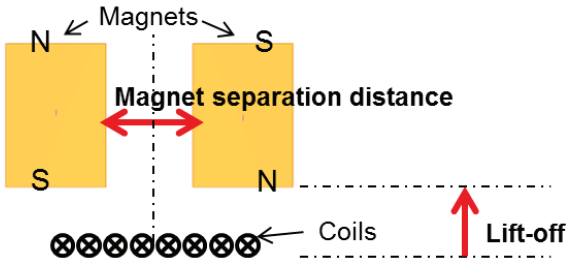

FIGURE 3. Geometric parametrization of the probe parts relatively to each other.

Having defined parameters to describe our study, we can now approach the problem with a qualitative analysis. Using the simulation models of the CIVA software, we have modeled the combined effect of both parameters when they simultaneously take low or high values. The results of our simulations are displayed in Fig. 4. The magnetic field generated by the magnetic assembly (which is assumed to be constituted only of two permanent 1 Tesla magnets in the simulation) is computed in the region located below the coils and visualized using a combination of isosurfaces and oriented vectors. In case (a), where the magnets are close to each other and close to the coils, the magnetic field is strong in the region where the eddy currents will be induced by the coils. However, the oriented vectors show that an important part of the magnetic field orientation is vertical and therefore not useful for longitudinal wave generation along the vertical direction denoted as z in the figure. In case (b), where the magnets are rather far from each other, we can clearly see that the magnetic field is almost exclusively horizontally polarized along the y axis in the figure. The drawback in this case is that the amplitude of the field is much lower in the region of interest than in the previous case. This leads us to the insight that the optimal way of positioning the magnetic assembly on top of our etched coils is a tradeoff between amplitude and horizontality of the magnetic field with the goal of generating the best possible acoustic wave field in the liquid sodium.

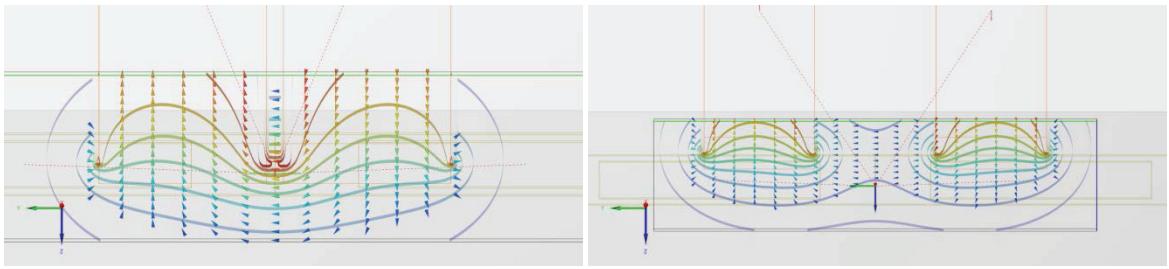

(a) (b)

FIGURE 4. Effect of low separation distance and lift-off (a) and high separation and lift-off (b) on the magnetic field and field lines (visualized with the help of vectors and isosurfaces).

The notion of "best possible wave field in the liquid sodium" has to be further defined to be used in practice. From the physical principles, we know that the EMAT probe generates a volumic time-dependent distribution of Lorentz forces. This volumic quantity can be transformed to a surface force, a stress field, given that the eddy currents are mostly localized close to the coils and exponentially decrease within the sodium (the so-called skin effect). Integration along the vertical axis, according to equation (1), is performed to obtain a vector stress field defined below the probe's contact surface with the liquid sodium.

$$\sigma = \int_{z=-\infty}^{z=0} J \times B dz \tag{1}$$

The simulation output is thus a two-dimensional region on which three stress components along directions *x*, *y* and *z* are defined. An example of a force field obtained by simulation is shown in Fig. 5.

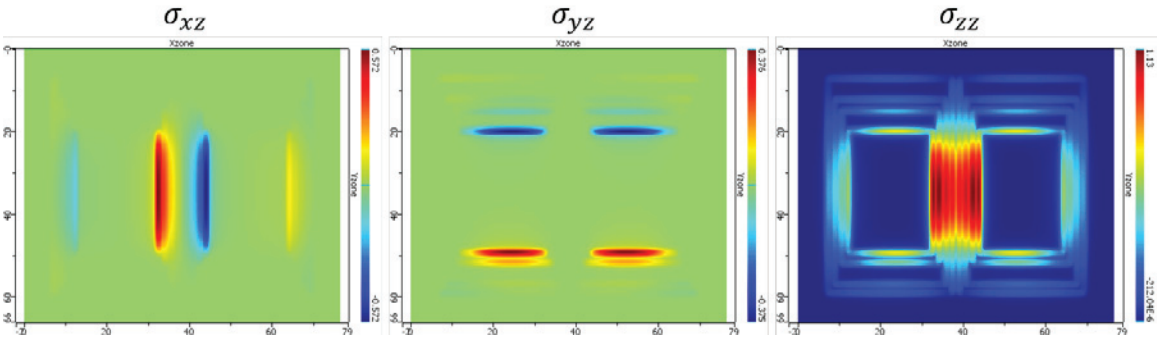

FIGURE 5. Example of the EMAT force field (from left to right: *x shear*, *y shear* and *z pressure* components) obtained by simulation with the CIVA model.

A quantitative evaluation criterion of the quality of the surface stress field introduced above is needed to compare parameter sets to each other and select an optimal set of parameters. Three criteria are introduced to this end: maximal amplitude of stress along z direction in the array aperture area (criterion 1), maximum amplitude of stress along z direction outside of array aperture area (criterion 2), ratio of maximum to minimum amplitude of Lorentz force along z direction over the 8 coils constituting the phased array in aperture area (criterion 3). These criteria are illustrated by Fig. 6. In this figure the locations of the maxima and the array aperture area are highlighted.

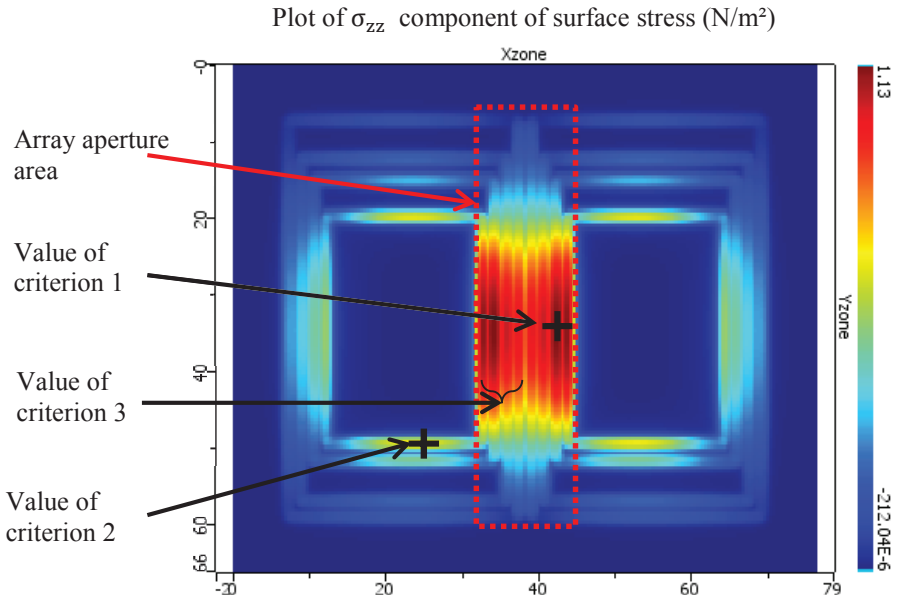

FIGURE 6. Criteria chosen for evaluating simulated stress distributions: maximum amplitude in array aperture area (criterion 1), maximum amplitude amplitude outside of array aperture area (criterion 2), ratio of maximum to minimum amplitude of Lorentz force along z direction over the 8 coils constituting the phased array in aperture area (criterion 3).

Now that the discriminating criteria for our study have been introduced, we can move on and define the input parameter space that we want to explore. Due to the dimensions of the magnets we will use during laboratory work, we choose to limit the magnet separation parameter to values in the range [10 mm, 70 mm]. The lift-off parameter was arbitrarily chosen to be in the [0.5 mm, 5 mm] range. The two dimensional region delimited by these two ranges is discretized into a 100 value cartesian grid, every node of this grid being a configuration of interest. A simulation is run on each configuration, the surface stress extracted and the three criteria computed and mapped to a 2D image. Following the first analysis, the parameter space was refined to the ranges [15 mm, 30 mm] and [0.5 mm, 5 mm] for magnet separation and lift-off respectively. The map of the three criteria obtained is shown in Fig. **7**. As one can see, the picture painted by each criterion is different. For example, if we analyze the results of the maximum force, we can see that two zones are good candidates: a small lift-off, small distance between magnets range and a high lift-off, small distance between magnets range. This is explained qualitatively by the Lorentz force generation process: high amplitude can be achieved by an intense static magnetic field (first case) or a very horizontal magnetic field (second case, the field lines are horizontal in the far field, which is when the magnets are lifted high above the coils, as in Fig. 4 b). Concerning the maximum force outside of the target area (criterion 2), some observations can also be readily made: when the distance between the two magnets is in the highest range, they are actually located above the looping part of the coils, effectively generating Lorentz forces only outside of the target region. These forces are minimized around a distance of 20 mm between magnets and for low lift-off values. Finally, looking at the last criterion, the ratio between the maximum and the minimum amplitude of the Lorentz force seen below the coils, there seems to be an L-shaped dependence pointing toward high separation distance and lift-off values. This again seems physical: the further away from the coils, the more in the far-field of the magnets will the specimen be, until it takes almost uniform values below the coils thus reducing the disparity between all elements of the probe.

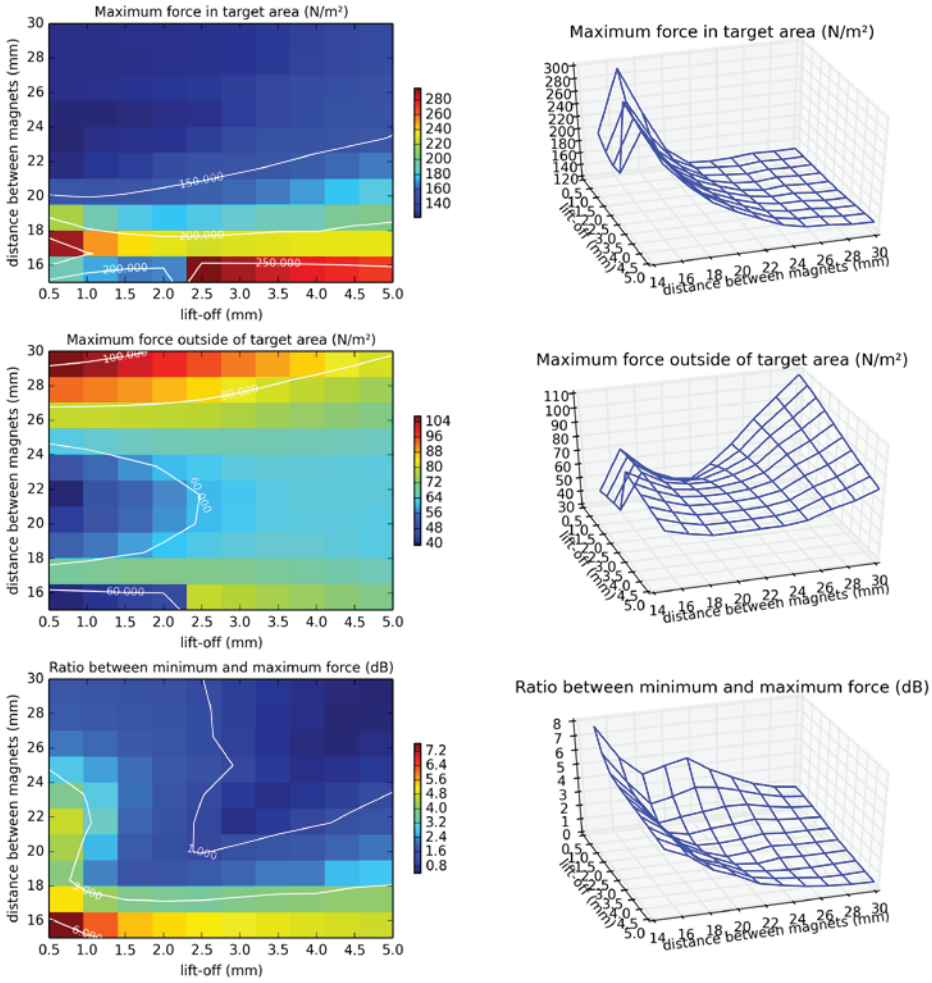

FIGURE 7. Maps of the three criteria over the simulated configuration space (from top to bottom). Each plot shows a two-dimensional map of the criterion as well as three dimensional meshing illustrating the topology of the response surface from the numerical simulation.

From the analysis of Fig. **7**, it is difficult to select an optimal configuration for the EMAT phased array probe due to the inherent tradeoffs between the different parameters. Therefore, we introduce a meta-criterion based upon the already defined criteria to ease the choice of the optimal configuration. We define this meta-criterion in equation (2), where c_i are the previously introduced criteria, c_i^0 are some physically relevant normalizing constants for criterion i and w_i are power law weights describing the importance of each criterion in the final solution.

$$c_{meta} = \sum_{i=1}^{3} \left(\frac{c_i}{c_i^0} \right)^{w_i} \tag{2}$$

In our case, the normalizing constants that were chosen are as follows: c_1^0 was equal to the maximal observed value of amplitude over the entire parameter space grid, c_2^0 was chosen to be equal to c_1^0, and c_3^0 was chosen to be equal to 6 dB. Different sets of weights lead to different mappings of the meta-criterion, as is demonstrated in Fig. 8. One can note that for criteria 2 and 3 the weights are negative. This is due to the fact that they have a detrimental impact on the Lorentz force generation process and should thus be minimized.

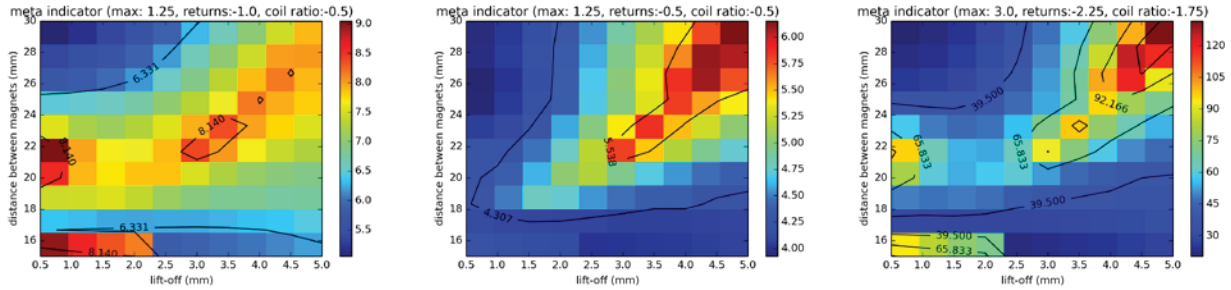

FIGURE 8. Three examples of values taken by the meta-criterion with three different sets of weights. Isosurfaces are shown at 90, 70, 50 and 30% of the maximum meta-criterion value found on the grid.

To select the magnet configuration used during the laboratory tests, the final weighting used was equal to $\left(c_1^0, c_2^0, c_3^0\right) = \left(1.5, -1.75, -1.75\right)$. The final map and the best resulting configuration are shown in Fig. 9.

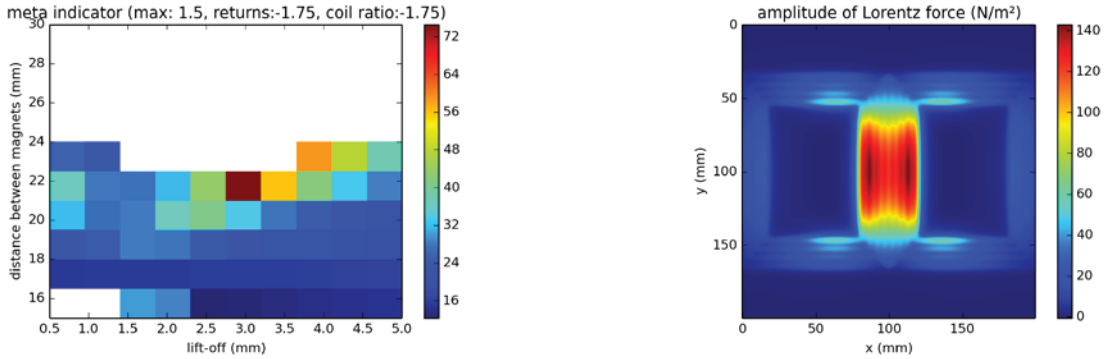

(a) (b)

FIGURE 9. Final optimization result: map of meta-criterion (a) and amplitude of Lorenz force for the optimal EMAT configuration selected for laboratory implementation (b).

To conclude this section, we used a magnet separation distance of 22 mm and a lift-off of 3 mm as the final parameter values for the EMAT phased array probe. In the next section, experimental results obtained with the assembled probe are described and analyzed.

EXPERIMENTAL SETUP OF THE PHASED ARRAY PROBE AND SIGNALS ON CALIBRATION BLOCK

Description of the Experimental Setup Used during Laboratory Testing

Once the optimal configuration was determined using the simulation assisted process described in the previous section, the magnetic circuit consisting of the two magnets and a ferrite element was assembled on top of the coils with the required magnet separation and lift-off distances. An electronic pulser was connected to the phased array probe and used to emit 300 V peak to peak pulses at 2 MHz to excite the coils. Emission and reception channel coils were soldered to different cables so as to be independent of each other. Finally, the acquisition mode was configured so that the received signal was averaged 16 times to increase the signal to noise ratio (SNR). A schematic of the setup is shown in Fig. 10.

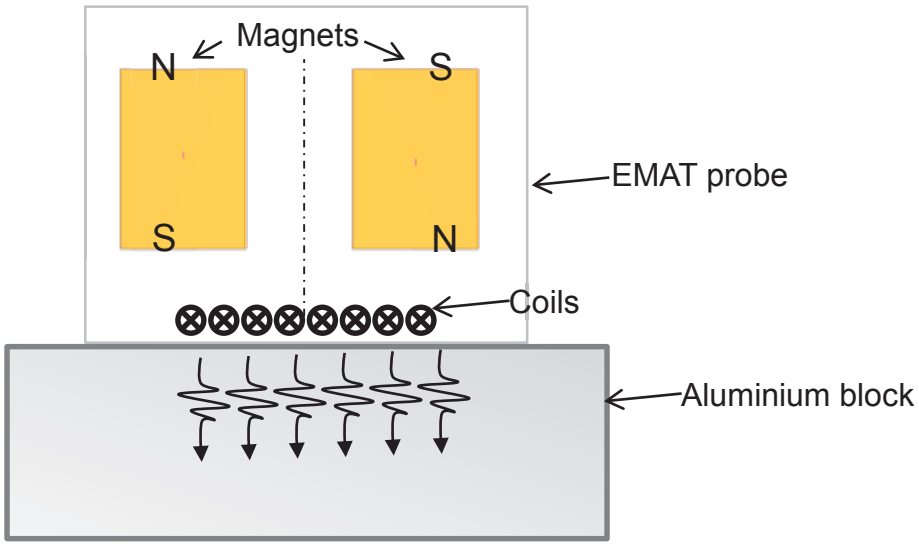

FIGURE 10. Experimental setup used during testing of the phased array EMAT probe.

Results for Normal Incidence Testing on Aluminium Block

Once the probe setup was in place, normal incidence testing was carried out to estimate elementary element sensitivities and sum the responses of the different elements to obtain an A-scan on the test aluminium block. The experimental result is shown in Fig. 11. The backwall echo obtained with this setup exhibited a SNR of 15 dB.

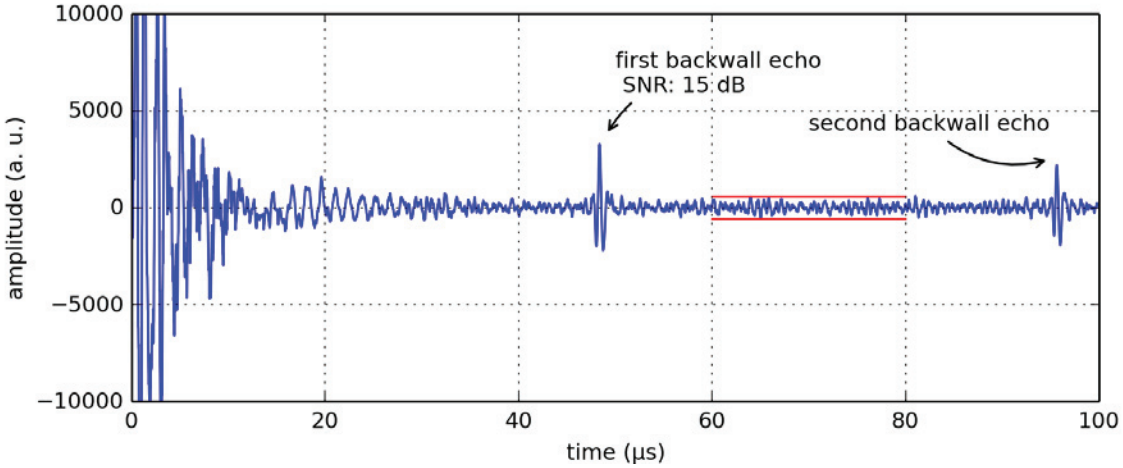

FIGURE 11. Experimental A-scan obtained with the newly designed phased array probe. The red colored region was used as a reference for the SNR measurement.

Results for Delay Law Testing on Aluminium Block

Following normal incidence testing, delay laws were applied to perform electronic sweeping at different angles with the EMAT phased array probe. To perform a deviation at angle θ delays in emission and reception have to be applied as following:

$$\tau_i^E = i\frac{p\sin\theta}{c_{Alu}} \tag{3}$$

$$\tau_i^R = -i\frac{p\sin\theta}{c_{Alu}} \tag{4}$$

In these equations p is the pitch of the phased array and c_{Alu} is the celerity of longitudinal waves in aluminium. The delay used for summing signals from channels i and j before computing the final signal is therefore:

$$\tau(i,j) = \tau_i^E + \tau_j^R \tag{5}$$

Using these equations, a sweeping B-scan was obtained as shown in Fig. 12. The amplitude variation shown by the echodynamic plot showcases the phased array's ability to deflect the generated ultrasonic waves.

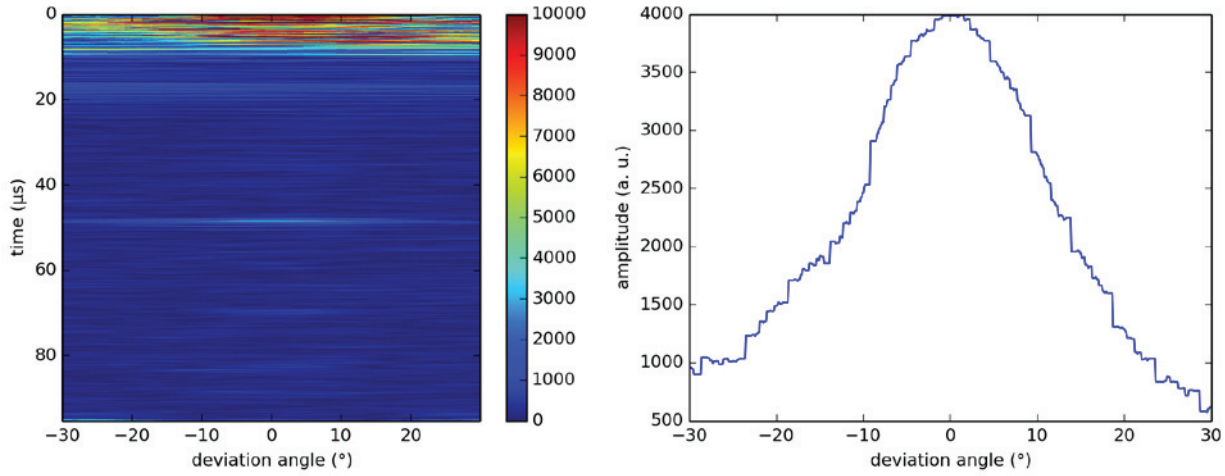

FIGURE 12. Angular scan obtained by applying electronic delay laws with the developed phased array probe and the associated echodynamic plot centered on the first backwall echo.

CONCLUSIONS

In this paper, we have described how we have optimized the design of an 8 element EMAT phased array probe by simulation and applied these results to obtain a functional probe in the laboratory. We concluded the design stage of this probe by choosing the geometry of the magnetic part of the probe in order to maximize the generation of Lorentz forces in liquid sodium. A simulation of the probe was conducted using CIVA software and led to an optimal solution by applying a multi-objective criterion to the Lorentz force field generated by the probe. The obtained solution was built using the existing probe parts and tested in the laboratory. A-scans were acquired in a longitudinal wave testing experiment on an aluminium block and proved satisfactory. To confirm the electronic sweeping capabilities of the probe, angular scanning between -30 and +30 degrees was also performed using longitudinal waves.

Perspectives for this work include laboratory tests on a drilled hole block and liquid sodium testing. Bigger phased array probe designs are also studied, in particular using 24 elements instead of 8.

ACKNOWLEDGMENTS

The authors would like to acknowledge the help of Quentin Élie and François Baqué while preparing the work presented in this article.

REFERENCES

1. F. Baqué, J.-M. Augem, J. Sibilo, and F. Reverdy, “Development of Tools, Instrumentation and Codes for Improving Periodic Examination and Repair of SFRs,” *Sci. Technol. Nucl. Install.*, **Vol. 2012**, May 2012.
2. J. P. Argous, M. Brunet, J. Baron, C. Lhuillier, and J. L. Segui, “Immersed acoustical transducers and their potential uses in LMFBR,” in *Second International Conference on Liquid Metal Technology in Energy Production*, pp. 4–23 (1980).
3. C. Lhuillier, O. Descombin, F. Baqué, B. Marchand, J.-F. Saillant, and J.-M. Ogem, “In sodium tests of ultrasonic transducers,” presented at the ANIMMA 2011, Ghent (2011).
4. Munemichi Kawaguchi, Akihiro Tagawa, and Shinya Miyahara, “Reactive Wetting of Metallic Plated Steels by Liquid Sodium,” *J. Nucl. Sci. Technol.*, **48**(4), 499–503 (2011).
5. H. M. Frost, "Electromagnetic-ultrasound transducers: principles, practice, and applications", *Academic Press*, (1979).
6. F. Le Bourdais and B. Marchand, “Design of EMAT Phased Arrays for SFR Inspection,” in *Review of Progress in Quantitative NDE*, **Vol. 33**, edited by D. O. Thompson, D. E. Chimenti, and L. J. Bond, published by AIP, Melville, NY, (2014).